Eur. Phys. J. D (2015) 69: 173
DOI: 10.1140/epjd/e2015-60200-y

THE EUROPEAN PHYSICAL JOURNAL D

Regular Article

Electron impact fragmentation of adenine: partial ionization cross sections for positive fragments*

Peter J.M. van der Burgt[1,a], Sinead Finnegan[1], and Samuel Eden[2]

[1] Department of Experimental Physics, National University of Ireland Maynooth, Maynooth, Co. Kildare, Ireland
[2] Department of Physical Sciences, The Open University, Walton Hall, Milton Keynes, MK7 6AA, United Kingdom

Received 29 March 2015 / Received in final form 4 June 2015
Published online 14 July 2015 –

Abstract. Using computer-controlled data acquisition we have measured mass spectra of positive ions for electron impact on adenine, with electron energies up to 100 eV. Ion yield curves for 50 ions have been obtained and normalized by comparing their sum to the average of calculated total ionization cross sections. Appearance energies have been determined for 37 ions; for 20 ions for the first time. All appearance energies are consistent with the fragmentation pathways identified in the literature. Second onset energies have been determined for 12 fragment ions (for 11 ions for the first time), indicating the occurrence of more than one fragmentation process e.g. for 39 u (C_2HN^+) and 70 u ($C_2H_4N_3^+$). Matching ion yield shapes (118–120 u, 107–108 u, 91–92 u, and 54–56 u) provide new evidence supporting closely related fragmentation pathways and are attributed to hydrogen rearrangement immediately preceding the fragmentation. We present the first measurement of the ion yield curve of the doubly charged parent ion (67.5 u), with an appearance energy of 23.5 ± 1.0 eV.

1 Introduction

Detailed knowledge of electron interactions with the DNA bases is important in order to understand and potentially model the nanoscale processes leading to radiation damage in biological material. As high-energy ionizing radiation passes through tissue, a large amount of secondary electrons (mainly below 30 eV) are produced along the tracks [1]. These secondary electrons play important roles in causing DNA strand breaks via excitation, ionization and dissociative electron attachment to the DNA components [2]. The resultant fragmentation mechanisms are particularly relevant in the context of radiation therapy, including ion beam cancer treatment [3,4]. Reviews of this field of molecular physics research can be found in references [5–11].

A number of studies of photon, ion and electron-induced dissociative ionization of gas-phase adenine have been carried out; the following overview highlights only those most closely related to the present work. Rice and Dudek [12] have measured a mass spectrum of adenine for 70 eV electron impact and have identified three of the main sequential fragmentation pathways. Occolowitz [13], Barrio et al. [14] and Sethi et al. [15] have measured mass spectra with isotope labeled adenines, showing that most of the fragmentation pathways exhibit largely random isotopic retention patterns, and that multiple pathways of successive fragmentations occur in parallel.

Minaev et al. [16] have measured the absolute total ionization cross sections of adenine for electron energies up to 200 eV as well as partial cross sections for the production of 24 fragment ions at 95 eV. They have proposed fragmentation patterns for the formation of the adenine ions with the help of quantum chemical calculations. Dawley et al. [17] have measured ion yield curves for 17 adenine positive ions for 5–20 eV electron impact using a quadrupole mass spectrometer. They have determined appearance energies for these ions and have compared these with quantum chemical calculations of the enthalpies of the possible reactions of the adenine positive ions.

A number of studies of adenine have been performed using photon impact and we briefly discuss two studies that are of direct relevance to the results presented in this paper. Jochims et al. [18] have studied photofragmentation of adenine using 6–22 eV synchrotron radiation. They have detected positive ions using a quadrupole mass spectrometer, and report appearance energies for 9 fragment ions. In combination with thermochemical data they have clarified fragmentation pathways. Pilling et al. [19] have studied photoionization of adenine using 12–21 eV synchrotron radiation in 1 eV steps and a time-of-flight mass spectrometer. They have obtained mass spectra by measuring photoelectrons and photoions in coincidence, and have determined the appearance energies of 5 fragment

* Contribution to the Topical Issue "COST Action Nano-IBCT: Nano-scale Processes Behind Ion-Beam Cancer Therapy", edited by Andrey Solov'yov, Nigel Mason, Gustavo García, Eugene Surdutovich.

[a] e-mail: peter.vanderburgt@nuim.ie

ions. The appearance energies will be compared with our measurements and those of Dawley et al. [17] later in this paper.

The focus of the present paper is on the production of positive ions by electron impact on isolated adenine molecules in the gas phase. Using computer-controlled data acquisition we have obtained 200 mass spectra in the range 0–100 eV with a step size of 0.5 eV. We report the first measurement of the ion yield curve of the doubly-charged parent in electron-impact mass spectrometry. From the mass spectra we have obtained the ion yield curves for most of the fragment ions, and have determined appearance energies for the singly and doubly charged parent ions and for 35 fragment ions. Ion yield curves are put on an absolute scale by normalizing their sum to the average of calculated total ionization cross sections. Appearance energies have been determined. A detailed discussion is given regarding multiple possible fragmentation pathways of adenine, including hydrogen rearrangement immediately preceding the fragmentation.

2 Experiment

A detailed description of the experimental set-up and the data analysis has been given by van der Burgt et al. [20] and only a brief overview will be given here. An effusive beam of adenine molecules is produced by heating an oven containing adenine powder (99% purity from Sigma Aldrich) to a temperature of 200 °C. Comparison of mass spectra taken just before and after the data acquisition shows no sign of thermal decomposition.

Adenine occurs in a number of tautomeric forms [21,22]. Touboul et al. [23] have performed VUV photoionization of gas phase adenine and have made a comparison between oven and aerosol vaporization showing that jet-cooling of vaporized adenine efficiently leads to the predominance of the most stable 9H-amino tautomer (ade-n9) in the beam. Plützer et al. [24,25] have performed IR-UV and R2PI double resonance spectroscopy of adenine, vaporized in an oven before expansion through the nozzle. The bands observed in their jet-cooled UV and IR adenine spectra are attributed to the 9H-amino tautomer. These findings are confirmed also by MP2 and density functional theory calculations. These authors state in their conclusion that without jet cooling, the IR spectrum is more complex most likely because of the presence of other tautomers. Based on these results we infer that our beam contains mostly the 9H-amino tautomer (see Fig. 1), but that other tautomers are likely present in smaller quantities.

In the mass spectra 136 u is weakly present but poorly resolved adjacent to the strong peak of the parent ion. The 136 u:135 u ratio is of the order of 0.05–0.08, in agreement with the expected isotope ratio of 7.3%. As protonated adenine is a well-known product of ionized adenine clusters [26], this result supports the absence of clusters in the present target beam.

The adenine beam is collimated by a skimmer and is crossed by a pulsed electron beam with a repetition rate of 8 kHz and a 1.0 μs pulse width. Positively charged product ions are extracted into a reflectron time-of-flight mass spectrometer. A delay generator is used to synchronise the pulsing of the electron gun, the ion extraction voltage, and the start of the multichannel scaler that is used to collect the counts from the microchannel plate detector.

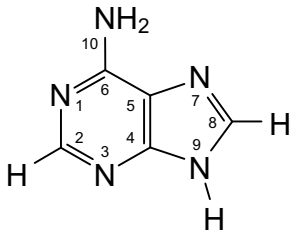

Fig. 1. Structure of the most stable 9H-amino tautomer (aden9) of adenine.

Data acquisition is controlled using a LabVIEW program, which increments the electron impact energy in 0.5 eV steps from 0 to 100 eV and acquires a mass spectrum at each energy. The full data set, collected in a 42 h period with 24 scans of the electron impact energy, is a two-dimensional array of ion yield as a function of time-of-flight and of electron impact energy. After each completed scan the data set is saved, and successive sets have been examined showing that the intensity of the adenine beam was constant during the experiment, and that there were no undesired effects during the data acquisition. As adjacent peaks above 20 u in the mass spectra are not fully resolved, ion yield curves have been extracted from the full data set by fitting groups of adjacent peaks with sequences of normalized Gaussians.

Appearance energies (first onsets) have been determined by fitting an onset function $f(E) = c(E-E_0)^p$ convoluted with a Gaussian to each of the ion yield curves. For second and third onsets additional terms were included in the onset function (for details see Ref. [20]). The fitting has been implemented in LabVIEW.

The presence of water in the vacuum system has not been fully eliminated, and for this reason the 16–18 u fragments are not considered in this paper. The yield curves for the 17 u and 18 u fragments have been compared with the recommended ionization cross sections for the production of H_2O^+ and OH^+ from [27] in the range 10–40 eV to obtain a calibration of the incident electron energy with an estimated error of ±0.3 eV.

3 Results and discussion

3.1 Total ionization cross section and normalization of the data

Tests performed with cytosine [28] have shown that the reflectron time-of-flight mass spectrometer has an ion collection and detection efficiency that is mass independent to good approximation. Because all data is extracted from a single data set, we have been able to obtain two curves

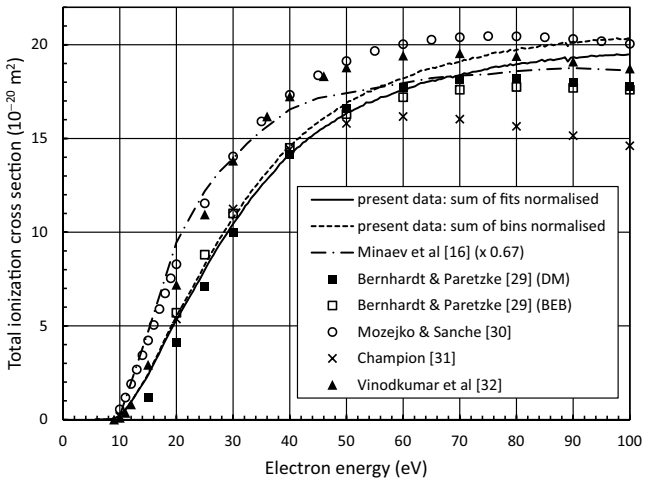

Fig. 2. Total ionization cross sections for electron impact on adenine. The lines indicate experimental results; the symbols are theoretical results. For more details see text.

for the total ionization cross section: (1) by adding all the ion yield curves, and (2) by summing all the counts collected in the mass spectra (excluding 16–18 u). The first curve has been normalized at 70 eV to the average of the theoretical cross sections [29–32] presented in Figure 2. The same normalization factor has been used for the second curve. We have obtained partial ionization cross sections by multiplying each ion yield curve with the same normalization factor.

The overall shape of our curve is in good general agreement with the theoretical ionization cross sections, although our curve rises slower than any of the theories. This could be partly due to a variation in the overlap of the electron beam and the adenine beam at low electron energies, but we note that our adenine measurement was done in between measurements for thymine [20] and cytosine [28], both of which show a somewhat better agreement with theory in the overall shapes of the curves. For easier shape comparisons in Figure 2, the absolute total ionization cross section measured by Minaev et al. [16] was multiplied by 0.67, such that it is also normalized to the average of the theoretical cross sections at 70 eV.

There are several contributions to the uncertainties in the partial ionization cross sections. Based on the standard deviation in the average of the five theoretical values at 70 eV, the uncertainty in the normalization is estimated to be 9.3%. An estimate for the statistical uncertainty in each ion yield curve is obtained by taking the standard deviation in the average ion yield from 90 to 100 eV (most ion yields are nearly constant in this energy region). This gives a statistical uncertainty of lower than 0.5% for partial ionization cross sections that are larger than 1.0×10^{-20} m^2 in the range from 90 to 100 eV, 0.5–1.2% for the range $(0.5–1.0) \times 10^{-20}$ m^2, 1.2–2.2% for the range $(0.2–0.5) \times 10^{-20}$ m^2, and higher than 2.2% for smaller partial ionization cross sections.

There are also uncertainties associated with the representation of each group of peaks by a series of Gaussians. Based on the fit results we estimate these to be lower than 2% for partial ionization cross sections that are larger than 1.0×10^{-20} m^2, 2–5% for the range $(0.5–1.0) \times 10^{-20}$ m^2, 5–10% for the range $(0.2–0.5) \times 10^{-20}$ m^2, and higher than 10% for smaller partial ionization cross sections.

Regarding the relative intensities of the fragment ions, we obtain reasonable overall agreement with the results of Rice and Dudek [12] at 70 eV, and with the results of Minaev et al. [16] at 95 eV. The only exceptions are for 28 u and 29 u: we obtain relative intensities of 81% and 18%, respectively, whereas Minaev et al. [16] obtain 21% and 8.6% (calculated using their table I). At 70 eV we obtain a relative intensity of 88% for 28 u, in reasonable agreement with 78% reported by Rice and Dudek [12] (read from figure 13). The 70 eV mass spectrum of Dawley et al. [17] shows a 28 u peak that is higher than the 135 u peak, indicating a relative intensity of about 130%. Perhaps this indicates that the presence of tautomers in the beams in different experiments has a big effect on the abundance of the 28 u fragment. Alternatively, differences like this may be related to the acceptance of the mass spectrometers, with relatively high kinetic energy fragment ions like CNH_2^+ particularly affected.

3.2 Appearance energies

Table 1 compares the appearance energies for the parent ion and a number of the fragment ions obtained by electron impact and by photoionisation using synchrotron ionisation. We have obtained 8.0 ± 0.2 eV for the parent ion, which is significantly lower than the recent values obtained by electron impact by Minaev et al. [16] and Dawley et al. [17], but is in agreement with the recent values obtained using synchrotron radiation by Jochims et al. [18] (see Tab. 1) and Touboul et al. [23] (8.267 ± 0.005 eV), and the calculated value of Minaev et al. [16] (7.98 eV). Trofimov et al. [33] have obtained 8.47 ± 0.02 eV using synchrotron radiation and calculated values in the range 7.87–8.58 eV using several theoretical methods. Other recent theoretical values have been obtained by Bernhardt and Paretzke [29] (8.48–8.65 eV), Champion et al. [31] (8.44 eV), Barbatti and Ulrich [34] (6.46–8.69 eV), Bravaya et al. [35] (8.13 eV), and Close and Øhman [36] (8.26–9.42 eV)

Regarding the appearance energies of the fragment ions, we note that all our appearance energies are in agreement with those of Jochims et al. [18] (only slightly outside the range of quoted error bars for 108 u), but there are several disagreements with the results of Dawley et al. [17] and Pilling et al. [19]. Pilling et al. [19] attribute the disagreement of their results with those of Jochims et al. [18] to the presence of higher harmonics in the synchrotron beam in reference [18]. Notably, all appearance energies of 28 u are in agreement, but there are clear disagreements for several of the main fragment ions such as 81 u, 70 u, and 54 u.

Figure 3 shows the appearance energies and higher onsets determined in the present work. This includes the first

Table 1. Comparison of presently measured fragment ion appearance energies with the available previous data for adenine. The uncertainties in the present data have been obtained directly from the non-linear fitting algorithm. Dawley et al. [17] report a second onset for 40 u at 18.5 ± 0.4 eV, which compares with 18.3 ± 1 eV obtained from the present data

Mass	Formula	Present data	Dawley et al. [17]	Jochims et al. [18]	Pilling et al. [19]
		electrons	electrons	photons	photons
135	$C_5H_5N_5^+$	8.0 ± 0.2	8.7 ± 0.3	8.2 ± 0.03	
108	$C_4H_4N_4^+$	11.3 ± 0.2	11.7 ± 0.2	11.56 ± 0.05	12.3 ± 0.1
107	$C_4H_3N_4^+$	13.7 ± 0.2	13.9 ± 0.3		
81	$C_3H_3N_3^+$	13.1 ± 0.2	14.1 ± 0.5	12.8 ± 0.1	12.4 ± 0.2
80	$C_3H_2N_3^+$	14.8 ± 0.7	15.1 ± 0.5		
70	$C_2H_4N_3^+$	12.6 ± 0.4	14.9 ± 0.2	13.1 ± 0.1	13.8 ± 0.3
67	$C_3H_3N_2^+$	13.2 ± 0.7	15.6 ± 0.3		
66	$C_3H_2N_2^+$	13.5 ± 0.2	14.2 ± 0.3	13.2 ± 0.1	
65	$C_3HN_2^+$	15.7 ± 1.3	17.9 ± 0.4		
54	$C_2H_2N_2^+$	13.5 ± 0.3	14.6 ± 0.3	13.7 ± 0.1	14.4 ± 0.3
53	$C_2HN_2^+$	15.3 ± 0.6	16.7 ± 0.5		
43	$CH_3N_2^+$	13.3 ± 0.6	14.0 ± 0.3	13.0 ± 0.1	
40	CN_2^+	15.9 ± 0.2	15.7 ± 0.3		
39	C_2HN^+	17.1 ± 0.5	18.1 ± 0.2		
29	CH_3N^+	13.7 ± 0.3	15.15 ± 0.15	14.0 ± 0.1	
28	CH_2N^+	12.9 ± 0.4	13.1 ± 0.5	13.1 ± 0.1	12.9 ± 0.3
27	CHN^+	14.0 ± 0.6	13.5 ± 0.2		

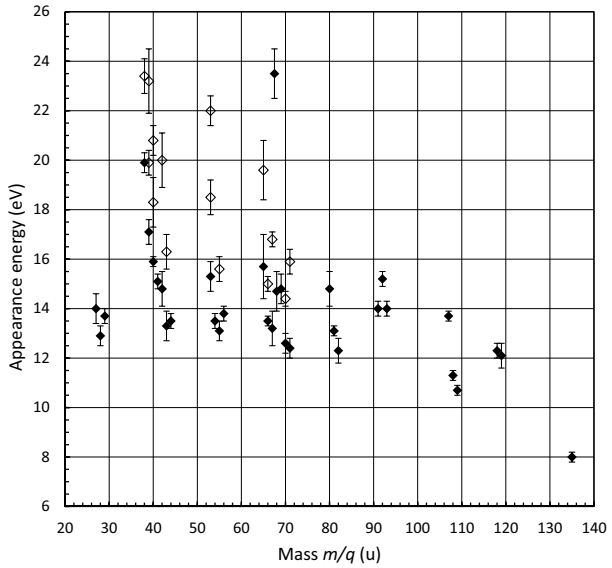

Fig. 3. Appearance energies for positive fragment ions of adenine. For each fragment, the lowest onset is shown as a solid diamond, and higher onsets are shown as open diamonds.

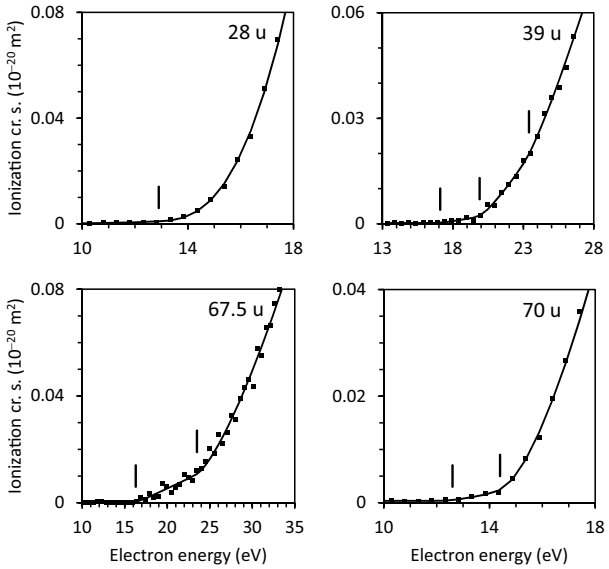

Fig. 4. Partial ionization cross sections of four selected adenine fragments. The appearance energies, second and third onsets, and fitted onset functions are also shown.

measurements of appearance energies for 20 fragment ions. The appearance energies of 12 u, 13 u and 14 u (not shown in Fig. 3) are 25 ± 2 eV, 26.5 ± 1.2 eV, and 19.6 ± 1.1 eV, respectively. Further examples of new appearance energies are 13.7 ± 0.3 eV for 29 u, 13.5 ± 0.3 eV for 44 u, 12.4 ± 0.4 eV for 71 u, 15.2 ± 0.3 eV for 92 u, and 12.1 ± 0.5 eV for 119 u. The appearance energy of the doubly-charged adenine parent ion at 67.5 u is 23.5 ± 1.0 eV (see discussion in Sect. 3.3.6).

All appearance energies we observe are consistent with the sequential fragmentation pathways discussed in the literature (for an overview see Fig. 5 in Jochims et al. [18] and Scheme I in Sethi et al. [15]). This is contrary to the appearance energies obtained by Dawley et al. [17], which exclude a near-threshold formation of 43 u by HCN loss from 70 u, and a near-threshold formation of 27 u by HCN loss from 54 u. We note that taking the estimated errors into account, the appearance energies for 81 u and for 54 u overlap, and also for 54 u and 27 u. Our second onset in the 70 u ion yield at 14.4 ± 0.3 eV is in agreement with the appearance energy of Dawley et al. [17].

Four fits of appearance energies are shown in Figure 4. Almost all fits of the appearance energies yield curves with powers $p > 1$ and for the 27 u, 28 u, 29 u, 54 u, 80 u, 81 u,

108 u and 135 u ions powers $p \geqslant 2$ are obtained. This includes all the ions in the HCN-loss sequence, and also the prominent 28 u ion. We do not see any indication for second onsets in the ion yield curves of these ions. For these ions the ion yield just above the appearance energy is very low, affecting the quality of the fit of the onset function. We suspect that this may be part of the reason for the disagreements in Table 1. However, the appearance energies of 28 u are in good agreement, even though the fit of the onset function in our data yields $p = 2.6 \pm 0.3$.

A high value of p could indicate that there are several onsets very close to each other due to the presence of several fragmentation pathways with similar appearance energies. Studies with isotope labeled adenines [13–15] show that most of the fragmentation pathways exhibit largely random isotopic retention patterns, indicating the presence of multiple fragmentation pathways. Based on this we attribute the rapid rise of these ion yields, with powers $p \geqslant 2$, to several onsets very close to each other due to the presence of parallel fragmentation pathways with similar appearance energies.

The energy differences between the first and second onsets range from 1.5 to 5.2 eV, e.g. 2.8 ± 1.0 for 39 u, 5.2 ± 1.8 eV for 42 u, 1.5 ± 0.5 for 66 u, and 1.8 ± 0.7 eV for 70 u. This is clearly too high to be linked to the rearrangement of one or two hydrogen atoms, and we conclude that there must be distinctly different fragmentation processes occurring for the fragments for which we observe a second onset.

3.3 Fragmentation pathways

Previous research has clearly shown that there are multiple pathways of successive fragmentations occurring in parallel, which lead to formation of fragment ions of the same mass but with atoms from different locations in the parent molecule via different pathways. Minaev et al. [16] state that there are independent parallel-successive schemes of fragmentation. Sethi et al. [15] conclude from studies with isotope labeled adenines that most of the fragmentation pathways exhibit largely random isotopic retention patterns, and that deuterium labeling is inconclusive because of rearrangements of hydrogen prior to expulsion of HCN. The studies of Barrio et al. [14] with ^{15}N labeled adenines combined with the results of Sethi et al. [15], show that the formation of 108 u by HCN loss is over 90% site specific for N1 and C2 and 6–8% for C2 and N3. Contrary to this, the populations of M-2(HCN) ions (81 u) and of M-HCN-NH_2CN ions (66 u) originate from pathways involving initial HCN loss from all the five nitrogen atoms in the molecule. These studies also show that fragmentation is initiated predominantly by breakage of the pyrimidine ring. In the following paragraphs we briefly discuss the fragmentation pathways and present some new insights that the present data provides.

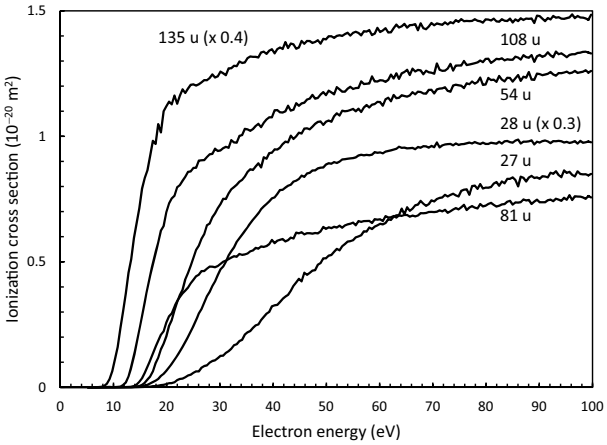

Fig. 5. Partial ionization cross sections of the parent ion (135 u) and the 108 u, 81 u, 54 u, 28 u, and 27 u fragments of adenine.

3.3.1 Formation of 108, 81, 54 and 27 u by successive HCN loss

Subsequent loss of HCN or CNH groups (reactions 1–4 in Ref. [18], route 4 in Ref. [16]) has been identified as the principal fragmentation pathway of adenine, resulting in ions of mass 108 u, 81 u, 54 u and 27 u. Consistent with this, the appearance energies of these ions are successively higher. The partial ionization cross sections for these ions are shown in Figure 5. It is seen that the curves are all different in shape and are all rising rapidly within the first 10 eV above threshold, with the exception of the 27 u curve, which rises more slowly. Above 70 eV the 81 u yield is lower than the 54 u and 27 u yields.

Studies with isotope labeled adenines [14,15] show that the first loss of HCN is over 90% site specific for the N1 and C2 atoms, but that the populations of 81 u and 54 u ions originate from pathways involving initial HCN loss from all the five nitrogen atoms in the molecule. The 81 u, 54 u and 27 u ion yield curves have no multiple onsets, which indicate that the various fragmentation pathways leading to these ions must have very similar appearance energies, which are not resolved in the present experiment. As discussed in Section 3.2, the ion yields for all ions in the HCN-loss sequence rise very rapidly just above threshold with powers $p \geqslant 2$, which may indicate the presence of two or more onsets very close to each other.

3.3.2 Formation of 107, 80 and 53 u

Different pathways have been suggested for the formation of these ions. Jochims et al. [18] (reactions 11–13) have suggested that these ions are formed by H_2CN loss from the parent ion, followed by successive loss of two HCN groups. Sethi et al. [15] have suggested that these ions are formed by H loss from 108, 81 and 54 u. Minaev et al. [16] attribute the formation of 80 u to a breakage of the C2-N3 and C5-C6 bonds (route 2 in Ref. [16]). All these suggestions are consistent with the successively higher appearance energies we observe for these fragment ions. Given

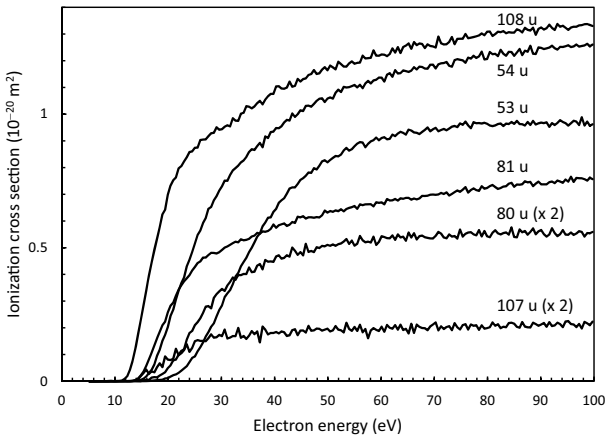

Fig. 6. Partial ionization cross sections of the 108 u, 107 u, 81 u, 80 u, 54 u and 53 u fragments of adenine.

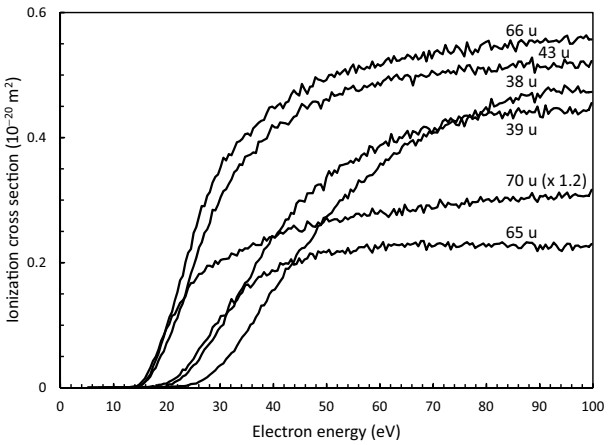

Fig. 7. Partial ionization cross sections of the 70 u, 66 u, 65 u, 43 u, 39 u and 38 u fragments of adenine.

the quoted uncertainties the appearance energies for 80 u and for 53 u overlap.

The partial ionization cross sections are shown in Figure 6 and provide additional information. The 107 u and 108 u partial ionization yields have similar shapes and the yield ratio 107 u: 108 u varies only slowly from 0.090:1 at 30 eV to 0.080:1 at 60 eV and is constant above that. We interpret this as being due to a possible rearrangement of a hydrogen atom immediately preceding the fragmentation leading to either HCN loss or H_2CN loss. In clear contrast to this, the partial ionization cross sections for 80 u and 81 u have very different shapes, and the same holds for 53 u and 54 u. This indicates that the relative importance of the different pathways suggested is different for each of these ions (107, 80 and 53 u).

We note here that below 40 eV the ion yield curves for 54, 55 and 56 u are different with somewhat different appearance energies, but above 40 eV the yield ratio becomes constant and is 54 u:55 u:56 u = 1:0.20:0.14, possibly indicating the rearrangement of one or two hydrogen atoms immediately preceding the fragmentation. 55 u could therefore be due to CN loss from 81 u.

3.3.3 Formation of 28 u

Apart from the parent ion, the most prominent peak in the mass spectrum is 28 u. Its partial ionization cross section is shown in Figure 5. This fragment has been identified as CH_2N^+, resulting from two possible two-bond dissociation routes (reaction 10 in Ref. [18], routes 1 and 3 in Ref. [16]) from the parent ion. The composition of 28 u is exclusively CH_2N^+, with an effectively random distribution of N atoms [15], indicating the existence of other pathways.

The appearance energy of 28 u of 12.6 ± 0.3 eV is quite low, but this does not exclude the possibility of formation by successive fragmentation via 70 u, or 108 u. There is no indication for a second onset in the ion yield curve (see Figs. 4 and 5), but the value of the exponent in the fitting of the appearance energy is $p = 2.6 \pm 0.3$, which shows that the ion yield rises very rapidly in the first 2 eV above threshold and which is possibly due to multiple pathways with very similar appearance energies.

3.3.4 Formation of 66 u and 39 u

The partial ionization cross sections for these ions are shown in Figure 7. Loss of NH_2CN from the $C_4H_4N_4^+$ fragment ion, followed by loss of HCN has been identified as a possible path for the formation of 66 u and 39 u (reactions 5 and 6 in Ref. [18]). Sethi et al. [15] conclude that the main population of 66 u ions is not derived from M-HCN-NH_2CN in which N1 and C2 are lost in the first step. The appearance energies for 93 u (14.0 ± 0.3 eV) and 66 u (13.5 ± 0.2 eV) (nearly) exclude the opposite succession M-NH_2CN-HCN for the formation of 66 u. This indicates that 66 u originates from a HCN loss in the first step that involves other C and N atoms. A second onset in the 66 u ion yield curve indicates also that more than one fragmentation process is involved in the formation of this ion. The ion yield curve of 39 u (Fig. 4) shows a second and a possible third onset, also indicating formation via multiple fragmentation pathways.

3.3.5 Formation of 70 u and 43 u

The partial ionization cross sections for these ions are shown in Figure 7. The 70 u and 43 u peaks appear distinctively next to the 64–67 u and 38–41 u groups in the mass spectra, strongly suggesting a separate fragmentation pathway involving C_3HN_2 loss followed by HCN loss (reactions 7 and 8 in Ref. [18]). Jochims et al. [18] and Minaev et al. [16] suggest that 70 u could also be formed by C_2N loss from 108 u (reaction 9 in Ref. [18]). However, Sethi et al. [15] did not find any detectable precursor of 70 u and uniquely identified the skeletal atoms of this fragment as N1-C2-N3-C4-N9.

The 70 u ion yield curve shows an appearance energy at 12.6 ± 0.4 eV and a second onset at 14.4 ± 0.3 eV, indicating

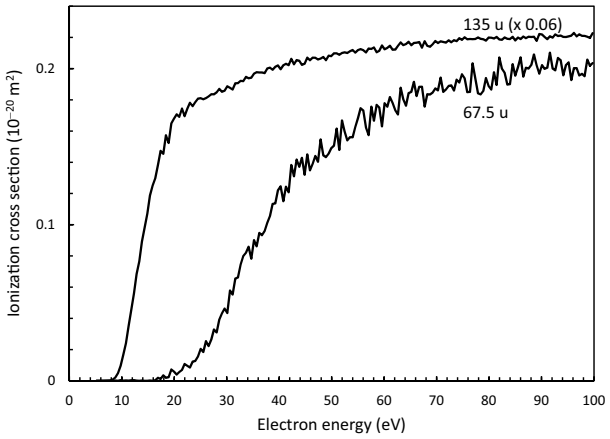

Fig. 8. Partial ionization cross sections of the singly charged (135 u) and the doubly-charged (67.5 u) adenine parent ions.

the existence of two pathways for the formation of this ion. We note that Figure 2d in Jochims et al. [18] clearly shows an appearance energy at 13.1 eV and a second onset at 14.1 eV. As can be seen in Figure 4, the 70 u ion yield in the range 12.6–14.4 eV is quite low, showing that the probability for the first pathway must be low. The second onset is possibly due to the pathway via 108 u, because this requires the rupture of an extra bond.

The 43 u ion yield curve shows an appearance energy at 13.3 ± 0.6 and a second onset at 16.3 ± 0.7 eV. The second onset is not very prominent, but the fit with an onset function containing two onsets is slightly better than the fit with one onset. The two fragmentation pathways suggested in the literature (via 70 u or via 108 u) would be expected to have similar thresholds, so it is not clear what fragmentation could be responsible for this second onset.

The higher appearance energies of 42 u and 41 u indicate that these ions could be formed by the successive loss of one and two hydrogen atoms from 43 u.

3.3.6 Formation of 67.5 u

Fitting of a sequence of normalized Gaussians to the 64–71 u group of peaks clearly showed that a peak at 67.5 u had to be included in the fit. This peak is attributed to the doubly charged parent ion. We do not see any indications of other doubly-charged fragments in our mass spectra.

Figure 4 shows that the Gaussian fitted feature at 67.5 u begins at 16.3 ± 0.5 eV, with a second onset at 23.5 ± 1.0 eV. 16.3 eV is evidently too low for double ionisation. Therefore we attribute this first onset to a background associated with the difficulty of using the Gaussian fitting function to separate weak features with half-integer difference in mass/charge. We assign the clear second onset at 23.5 ± 1.0 eV to the threshold for doubly charged adenine. This interpretation is consistent with the absence of a 67.5 u feature in earlier photo-ionization mass spectra recorded up to 22 eV [18,19]. The mass spectrum of adenine at 70 eV electron impact [12] shows the presence of 67.5 but this is not discussed by the authors. No previous appearance energies for doubly charged nucleobases have been reported in the literature. The present result is consistent with other molecules that have similar single ionization energies to adenine, for example toluene with single ionization at 8.81 ± 0.03 eV and double ionization at 23.81 ± 0.06 eV [37].

Doubly-charged adenine has been clearly observed by Alvarado et al. [38] in adenine mass spectra after collisions with 14 keV projectiles (H^+ and H, He^+ and He, and C^+ and C), and by Bredy et al. [39,40] after impact with 3 keV Cl^+ ions and 36 keV F^{2+} ions.

We have examined the mass spectra of the other nucleobases measured in our laboratory, but do not observe any clear indications for the formation of doubly charged parent ions in these.

3.3.7 Formation of 118–120 u and 91–93 u

Loss of NH_3 or NH_2 leading to 118 and 119 u, followed by HCN loss to 91 and 92 u has been identified by Sethi et al. [15] as a possible pathway, and NH loss is another possibility. The yields for these ions are very low, showing that this is only a minor fragmentation pathway. The partial ionization cross sections for these ions (not shown in this paper) have very similar shapes. Above 25 eV, the yield ratios are 118 u:119 u:120 u = 0.85:1:0.25 and 91 u:92 u = 0.40:1. However, the yield ratio 92 u:93 u is not constant, but varies from 1:0.48 at 30 eV to 1:0.53 at 100 eV.

We attribute these constant yield ratios to tautomerization (H atom rearrangements) preceding the fragmentation, although the presence of adenine tautomers in the molecular beam could also contribute. Constant yield ratios have also been observed several of the ion yield curves for cytosine [28].

4 Conclusion

We have presented substantial new information about the formation of positive fragment ions by low-energy electron impact on adenine in the form of ion yield curves, partial ionization cross sections and appearance energies. All appearance energies determined are consistent with the adenine fragmentation pathways discussed in the literature (for an overview of pathways see Fig. 5 in Jochims et al. [18] and Scheme I in Sethi et al. [15]).

Several groups of fragments (118–120 u, 107–108 u, 91–92 u, and 54–56 u) have ion yield curves with very similar shapes above 25 or 40 eV. We attribute these constant yield ratios to H atom rearrangements (tautomerization) immediately preceding the fragmentation, but the presence of tautomers in the molecular beam might also contribute to this

Appearance energies (first onsets) have been determined for 37 ions. The present work provides the first appearance energies for 20 fragment ions for which the

specific production pathways have not yet been explored in detail.

For 27, 28, 29, 54, 80, 81, 108 and 135 u, the ion yields rise very rapidly just above threshold with powers $p \geqslant 2$. We have attributed the rapid rise of these ion yields to several onsets very close to each other due to the presence of parallel fragmentation pathways with similar appearance energies.

Second onset energies have been determined for 12 fragment ions with energy differences between the first and second onsets range from 1.5 to 5.2 eV. We conclude that there must be distinctly different fragmentation processes producing these fragments.

We have presented the first measurement of the ion yield curve of the doubly charged parent ion, with an appearance energy of 23.5 ± 1.0 eV. The absence of discernible signals for doubly charged ions of the other nucleobases in mass spectra measured in our laboratory suggests that doubly charged adenine has a relatively high stability, with implications for its relative sensitivity to high energy radiation.

The authors are indebted to Dr. Stephan Denifl for discussions on the appearance energies of adenine and for providing the data from Dawley et al. [17]. The authors gratefully acknowledge financial support for scientific visits received from the Nano-IBCT project (COST Action MP1002) funded by the European Union. S. Eden acknowledges the support of the British EPSRC (EP/J002577/1 and EP/L002191/1).

References

1. A. Munoz, F. Blanco, G. Garcia, P.A. Thorn, M.J. Brunger, J.P. Sullivan, S.J. Buckman, Int. J. Mass Spectrom. **277**, 175 (2008)
2. B. Boudaïffa, P. Cloutier, D. Hunting, M.A. Huels, L. Sanche, Science **287**, 1658 (2000)
3. E. Surdutovich, A.V. Solov'yov, Europhys. News **40**, 21 (2009)
4. E. Surdutovich, A.V. Solov'yov, Eur. Phys. J. D **68**, 353 (2014)
5. H. Hotop, M.-W. Ruf, M. Allan, I.I. Fabrikant, Adv. At. Mol. Opt. **49**, 85 (2003)
6. R. Balog, J. Langer, S. Gohlke, M. Stano, H. Abdoul-Carime, E. Illenberger, Int. J. Mass Spectrom. **233**, 267 (2004)
7. L. Sanche, Eur. Phys. J. D **35**, 367 (2005)
8. I. Baccarelli, I. Bald, F.A. Gianturco, E. Illenberger, J. Kopyra, Phys. Rep. **508**, 1 (2011)
9. B.A. Huber, C. Malot, A. Domaracka, Y.A. Gauduel, A. Solov'yov, J. Phys.: Conf. Ser. **373**, 011001 (2012)
10. *Radiation Damage in Biomolecular Systems*, edited by G. García Gómez-Tejedor, M.C. Fuss (Springer, 2012)
11. M.A. Smialek, P. Limao-Vieira, N.J. Mason, A.V. Solov'yov, Eur. J. Phys. D **68**, 312 (2014)
12. J.M. Rice, G.O. Dudek, J. Am. Chem. Soc. **89**, 2719 (1967)
13. J.L. Occolowitz, Chem. Commun. 1226 (1968)
14. M.C.G. Barrio, D.I.C. Scopes, J.B. Holtwick, N.J. Leonard, Proc. Natl. Acad. Sci. USA **78**, 3986 (1981)
15. S.K. Sethi, S.P. Gupta, E.E. Jenkins, C.W. Whitehead, L.B. Townsend, J.A. McCloskey, J. Am. Chem. Soc. **104**, 3349 (1982)
16. B.F. Minaev, M.I. Shafranyosh, Yu. Yu Svida, M.I. Sukhoviya, I.I. Shafranyosh, G.V. Baryshnikov, V.A. Minaeva, J. Chem. Phys. **140**, 175101 (2014)
17. M.M. Dawley, K. Tanzer, W.A. Cantrell, P. Plattner, N.R. Brinkmann, P. Scheier, S. Denifl, S. Ptasińska, Phys. Chem. Chem. Phys. **16**, 25039 (2014) (see also electronic supplement)
18. H.-W. Jochims, M. Schwell, H. Baumgärtel, S. Leach, Chem. Phys. **314**, 263 (2005)
19. S. Pilling, A.F. Lago, L.H. Coutinho, R.B. de Castilho, G.G.B. de Souza, A. Naves de Brito, Rapid Commun. Mass Spectrom. **21**, 3646 (2007)
20. P.J.M. van der Burgt, F. Mahon, G. Barrett, M.L. Gradziel, Eur. Phys. J. D **68**, 151 (2014)
21. C. Fonseca Guerra, F.M. Bickelhaupt, S. Saha, F. Wang, J. Phys. Chem. A **110**, 4012 (2006)
22. R.K. Singh, J.V. Ortiz, M.K. Mishra, Int J. Quant. Chem. **110**, 1901 (2010)
23. D. Touboul, F. Gaie-Levrel, G.A. Garcia, L. Nahon, L. Poisson, M. Schwell, M. Hochlaf, J. Chem. Phys. **138**, 094203 (2013)
24. Chr. Plützer, E. Nir, M.S. de Vries, K. Kleinermanns, Phys. Chem. Chem. Phys. **3**, 5466 (2001)
25. C. Plützer, K. Kleinermanns, Phys. Chem. Chem. Phys. **4**, 4877 (2002)
26. N.J. Kim, Y.S. Kim, G. Jeong, T.K. Ahn, S.K. Kim, Int. J. Mass Spectrom. **219**, 11 (2002)
27. Y. Itikawa, N. Mason, J. Phys. Chem. Ref. Data **34**, 1 (2005)
28. P.J.M. van der Burgt, Eur. Phys. J. D **68**, 135 (2014)
29. P. Bernhardt, H.G. Paretzke, Int. J. Mass Spectrom. **223-224**, 599 (2003)
30. P. Możejko, L. Sanche, Radiat. Environ. Biophys. **42**, 201 (2003)
31. C. Champion, J. Chem. Phys. **138**, 184306 (2013)
32. M. Vinodkumar, Ch. Limbachiya, M. Barot, M. Swadia, A. Barot, Int. J. Mass Spectrom. **339-340**, 16 (2013)
33. A.B. Trofimov, J. Schirmer, V.B. Kobychev, A.W. Potts, D.M.P. Holland, L. Karlsson, J. Phys. B **39**, 305 (2006)
34. M. Barbatti, S. Ullrich, Phys. Chem. Chem. Phys. **13**, 15492 (2011)
35. K.B. Bravaya, O. Kostko, S. Dolgikh, A. Landau, M. Ahmed, A.I. Krylov, J. Phys. Chem. A **114**, 12305 (2010)
36. D.M. Close, K.T. Øhman, J. Phys. Chem. A **112**, 11207 (2008)
37. J. Roithová, D. Schröder, J. Loos, H. Schwarz, H.-C. Jankowiak, R. Berger, J. Chem. Phys. **122**, 094306 (2005)
38. F. Alvarado, S. Bari, R. Hoekstra, T. Schlathölter, J. Chem. Phys. **127**, 034301 (2007)
39. R. Brédy, J. Bernard, L. Chen, B. Wei, A. Salmoun, T. Bouchama, M.C. Buchet-Poulizac, S. Martin, Nucl. Instrum. Methods Phys. Res. B **235**, 392 (2005)
40. R. Brédy, J. Bernard, L. Chen, G. Montagne, B. Li, S. Martin, J. Chem. Phys. **130**, 114305 (2009)